Journal of Solid State Electrochemistry (2022) 26:2247–2260
https://doi.org/10.1007/s10008-022-05237-4

ORIGINAL PAPER

Fabrication and characterization of Ag- and Cu-doped TiO_2 nanotubes (NTs) by in situ anodization method as an efficient photocatalyst

O. Zakir[1,2] · A. Ait Karra[1] · R. Idouhli[1] · M. Elyaagoubi[2] · M. Khadiri[1,2] · Burak Dikici[3] · A. Aityoub[1] · A. Abouelfida[1] · A. Outzourhit[2]

Received: 4 April 2022 / Revised: 7 June 2022 / Accepted: 29 June 2022 / Published online: 15 July 2022

Abstract

In this study, copper (Cu) and silver (Ag)–doped TiO_2 nanotubes were fabricated by in situ anodization method to improve their photocatalytic performance. The resulting nanotubes (NTs) were characterized by scanning electron microscopy (SEM), energy-dispersive X-ray spectroscopy (EDX), X-ray photoelectron spectroscopy (XPS), X-ray diffraction (XRD), Raman spectroscopy, and Mott-Schottky analysis. The SEM study shows the formation of NT structure and reveals that the doping does not affect the surface morphology. The XPS analysis proves that a mixture of Ag^0/Ag^+ and Cu^+/Cu^{2+} exists simultaneously on the surface of the Ag- and Cu-doped TiO_2 NTs, respectively. XRD and Raman spectroscopy analyses show that the doping shifted the anatase and rutile phase transformation and stabilized the anatase phase. The Mott-Schottky measurements demonstrate that the potential of the flat band shifted to negative values by doping. The prepared NTs were evaluated in methylene blue (MB) photodegradation under UV. The results reveal that the doped TiO_2 NTs were more efficient than pure TiO_2 NTs in the degradation of MB. The Cu-doped TiO_2 NTs exhibited excellent degradation efficiency of about 92.61% with a kinetic rat 0.0089 min^{-1}. Furthermore, the reusability studies showed that the photocatalysts are globally stable and efficient for the degradation of MB.

Keywords Electrochemical anodization · Photocatalysis · Photodegradation · Nanotubes · TiO_2 · XPS · Methylene blue

Introduction

Titanium dioxide is the most widely used semiconductor as a chemically stable, highly efficient, and relatively inexpensive photocatalyst [1]. The fabrication of TiO_2 with interesting morphologies and properties has recently attracted considerable attention. Various nanostructures of TiO_2 such as nanowire, nanoparticles, nanorods, nanosheets, nanotubes, and microspheres have been successfully synthesized [2–8].

Among these nanostructures, it is well known that ordered TiO_2 nanotube arrays with larger specific surface areas are a suitable structure in photocatalytic applications. However, the photocatalytic efficiency of TiO_2 is mainly limited by its large bandgap, the recombination of photogenerated electron–hole pairs, and their small lifetime [9, 10]. Recently, many efforts have been made, and different approaches have been developed to improve these limitations, such as doping of TiO_2 [11–13], coupling the TiO_2 with a semiconductor material with a narrow bandgap [14–17], decoration of TiO_2 with different noble metals [18], and surface photosensitization [19]. The doping process is the typical approach that has been widely applied to enhance the photocatalytic efficiency of TiO_2 [20]. A previous study revealed that doping with metal elements reduces the bandgap of TiO_2 to increase the number of photogenerated electron–hole pairs and the recombination rate of the photogenerated electron–hole pairs [21, 22]. Park et al. [23]. doped TiO_2 by divalent metals (Co^{2+}, Ni^{2+}, Cu^{2+}, and Zn^{2+}) and showed that Cu-doped TiO_2 and Zn-doped TiO_2 were highly interesting materials in the photodecomposition of methylene blue. Sangpour et al. [24] showed that

✉ O. Zakir
othmane.zakir@gmail.com

1 Laboratory of Applied Chemistry and Biomass, Department of Chemistry, Faculty of Science Semlalia, University Cadi Ayyad, BP 2390 Marrakech, Morocco

2 Laboratory of Nanomaterials for Energy and Environment, Department of Physics, Faculty of Science Semlalia, University Cadi Ayyad, BP 2390 Marrakech, Morocco

3 Department of Metallurgical and Materials Engineering, Faculty of Engineering, Atatürk University, 25240 Erzurum, Turkey

doping with Ag, Au, and Cu metal increases the photocatalytic activity of TiO_2 by improving the radical formation. They found that the photocatalytic efficiency increased from 40% for pure TiO_2 to 90%, 75%, and 50% for Cu-doped TiO_2, Au-doped TiO_2, and Ag-doped TiO_2, respectively. Only a few studies focused on the doping of TiO_2 NTs during the anodizing process in the literature [25–29].

This study reports a simple approach to fabricating Cu and Ag-doped TiO_2 NTs by anodizing of pure titanium in glycerol electrolyte containing ammonium fluoride. The effects of incorporating ions into TiO_2 NTs on their photocatalytic efficiency were investigated. The morphology and structure were studied by scanning electron microscopy (SEM), energy-dispersive X-ray spectroscopy (EDX), X-ray photoelectron spectroscopy (XPS), X-ray diffraction (XRD), and Raman spectroscopy. The electrical properties were studied by Mott-Schottky measurement. The effect of Cu and Ag doping on the photocatalytic activity of doped samples was evaluated by methylene blue (MB) degradation under UV irradiation.

Materials and method

Materials

Titanium foil (99.99% pure, 1 mm thick), glycerol (99.8%, anhydrous), NH_4F (98%), HNO_3 (99.98%), HF (40%), silver nitrate ($AgNO_3$), copper (II) sulfate ($CuSO_4$, $5H_2O$), benzoquinone (99.5%), isopropanol (99.0%), triethanolamine (98%), and methylene blue were purchased from Sigma-Aldrich (St. Louis, USA).

Fabrication of pure and doped TiO_2 NTs

The titanium foils were first polished with different emery paper sizes (from #1000 to #5000 grade), rinsed with distilled water, and then chemically etched by immersion in a mixture of HF and HNO_3 acids for 10 s. The mix's HF/HNO_3/H_2O ratio was 1:1:2 in volume [30]. The pure and doped TiO_2 NTs were synthesized by electrochemical anodization of titanium foils in a glycerol-based electrolyte solution containing NH_4F and distilled water. The conditions of anodization are described in detail in our previous paper [31]. Briefly, the anodization was performed in a two-electrode electrochemical device with a platinum foil as the cathode and pure titanium as the anode. The anodization was carried out under a constant voltage of 60 V for 60 min at a temperature of 25 ± 1 °C. The distance between anode and cathode was kept at 1 cm. The electrolyte bath composition used to elaborate the different samples is listed in Table 1. The electrolyte solution was magnetically stirred during the electrochemical reaction (250 tr/min). After anodization, the anodized samples were immediately washed in distilled water. To improve the crystallinity of the as-synthesized NTs, the as-formed samples were heat-treated in a muffle furnace at 600 °C for 2 h with a heating ramp of 10 °C/min [32].

Characterization

The morphology and composition of the TiO_2 NTs and modified TiO_2 NTs were characterized under a field emission scanning electron microscope (TESCAN VEGA3 SEM) coupled with an energy dispersive X-ray microanalysis system (EDAX, EDX) operated at an accelerating voltage of 20 kV and under a pressure of 1.3×10^{-4} Pa. The samples' surface properties and oxidation states were analyzed using X-ray photoelectron spectroscopy (XPS). The XPS peaks are deconvoluted using CasaXPS software (version 2.3.23) with Lorentzian Asymmetric LA (1.53, 243) peak fitting. The TiO_2 crystalline structure was determined by X-ray diffraction (XRD) using a Rigaku, SmartLab SE, operated at 40 kV and 50 mA. The X-ray source consists of Cu Kα radiation (1.54184 Å) selected with a Cu K_β filter. The data were collected between 10 and 70° with a scan speed of 5°/min. The Raman spectrum was recorded using a confocal Raman spectrometer (Confotec MR520 microscope) instrument with a laser ($\lambda = 532$ nm) and analyzed with 1200 lines/in the grating. The acquisition time of 30 s is used with 10 mW incident power. The functional groups and their modes of vibrations are analyzed by using a VERTEX 70 FT-IR Spectrometer with ATR attachment.

The Mott-Schottky measurements were performed using a conventional three-electrode cell in a 0.1 M Na_2SO_4 aqueous solution [33]. The anodized TiO_2 NT electrode (working area = 1 cm^2), a saturated calomel electrode (SCE), and a platinum sheet (4 cm^2) were used as the working, reference, and counter electrodes, respectively. The measurements were performed using a VoltaLab potentiostat (PGZ301) controlled by the VoltaMaster 4 software. The temperature was controlled in jacketed glass at 293 K using a bath

Table 1 The electrolyte used for the preparation of the samples

Samples	Electrolyte
Pure TiO_2 (TiO_2 NTs)	Glycerol + H_2O (8%) + NH_4F (0.4 M)
Cu doped TiO_2 (Cu-TiO_2 NTs)	Glycerol + H_2O (8%) + NH_4F (0.4 M) + $CuSO_4$, $3H_2O$ (0.2 M)
Ag doped TiO_2 (Ag-TiO_2 NTs)	Glycerol + H_2O (8%) + NH_4F (0.4 M) + $AgNO_3$ (0.2 M)

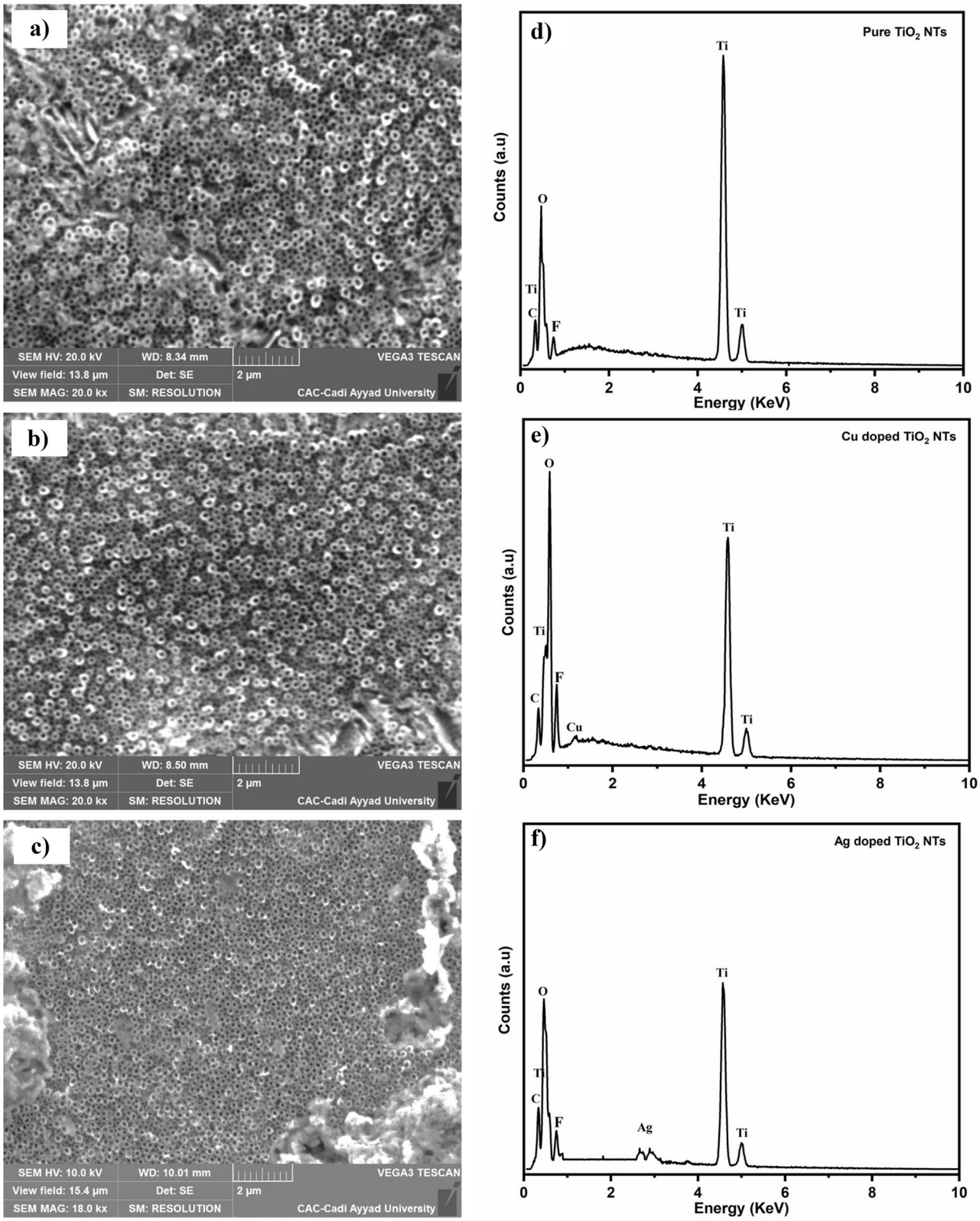

Fig. 1 SEM images and EDX spectra of pure TiO_2 NTs **a**, **d**, Cu-TiO_2 NTs **b**, **e**, and Ag-TiO_2 NTs **c**, **f**

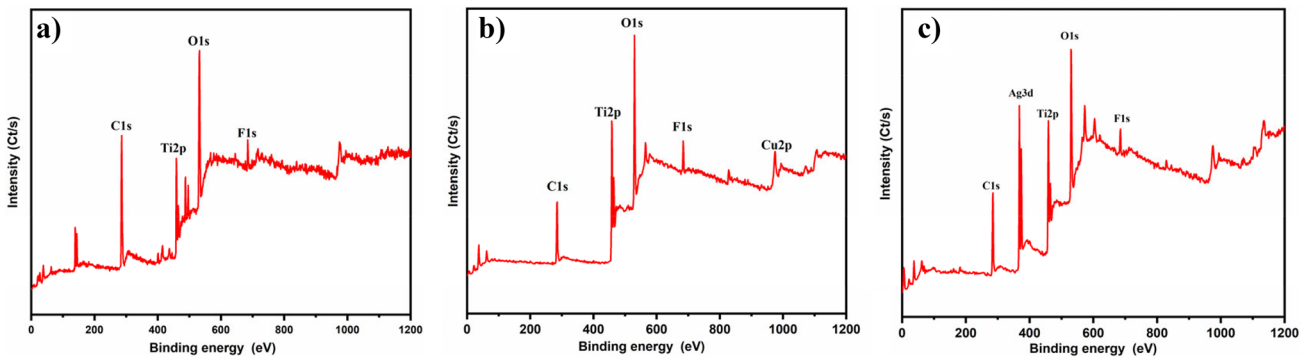

Fig. 2 Full XPS spectrum of **a** pure TiO_2 NTs, **b** Cu doped TiO_2 NTs, and **c** Ag-doped TiO_2 NTs

thermostat. The analysis was performed at a frequency of 1 kHz in a wide voltage range (from − 1 V to 1 V/SCE) [34].

Photocatalytic study

Photocatalytic activities of pure and doped TiO_2 samples were evaluated by degradation of the MB dye in an aqueous solution under UV irradiation. The initial concentration of MB was 2.5 mg/L. Before illumination, the TiO_2 NT photocatalyst was immersed in the reactor containing 50 mL of MB and magnetically stirred for 20 min in the dark to establish an adsorption–desorption equilibrium between the photocatalyst and MB. Then, the solution was irradiated under UV light using an Ultra-Vitalux lamp at 300 W with a high-pressure tungsten filament source for 4 h. The reactor temperature was kept at 25 °C by a water flow. At each 30-min interval, a volume of 3 mL of solution was sampled for analysis, and a UV–vis spectrophotometer measured the absorbance of MB at 664 nm. The reusability test was performed using the same protocol described above by reutilizing the used TiO_2 NT photocatalyst for the next experiment.

Results and discussion

Morphology and composition characterizations

Figure 1 shows a representative SEM image and EDX spectra of the pure TiO_2 NTs (Fig. 1a, d), Cu-TiO_2 NTs (Fig. 1b, e), and Ag-TiO_2 NTs (Fig. 1c, f). From SEM images, it can be seen that the morphology of the doped TNs is similar to that of pure TiO_2 NTs, indicating that these elements' doping does not influence the morphologies of the TiO_2. The highly ordered NT arrays with an inner diameter and wall thickness of about 127 and 52 nm, respectively, were produced on the titanium surface by anodization.

The EDX analysis was performed on the sample to verify the doping process and determine its surface's chemical composition. The EDX analysis indicates qualitatively the presence of the Ti, O, F, and C in all anodized samples. The peaks of copper (at 0.94 kV) and silver (at 2.98 kV) were also detected in the doped NTs, as revealed in Fig. 1e and f, respectively, indicating clearly that the doping has been carried out successfully.

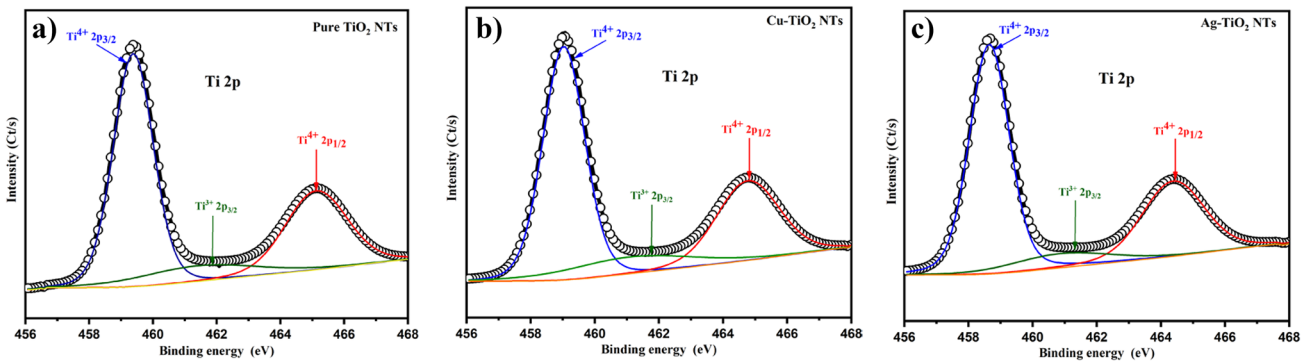

Fig. 3 Ti2p spectra: **a** pure TiO_2 NTs, **b** Cu-doped TiO_2 NTs, and **c** Ag-doped TiO_2 NTs

Table 2 Chemical composition of the Ag- and Cu-doped TiO_2 thin film surface

Samples	Position of peaks (eV)					Element (wt%)		Ratio O_L/O_H
	$Ti^{4+}2p_{3/2}$	$Ti^{4+}2p_{1/2}$	$Ti^{3+}2p_{3/2}$	O_L	O_H	Ti^{3+}	O_L	O_L/O_H
TiO_2 NTs	459.38	465.11	460.10	530.67	532.41	15.31	26.65	0.36
Ag-TiO_2 NTs	458.65	464.38	460.87	530.70	532.30	9.31	55.82	1.26
Cu-TiO_2 NTs	459.04	464.78	461.07	530.32	531.90	12.38	66.74	1.77

XPS analysis

The XPS analysis was performed to determine the composition and chemical bonding states of all samples. Figure 2 shows the survey spectra for pure and doped TiO_2 NTs. The photoelectron peaks for Ti, O, F, and C were clearly recorded for all three samples. The peaks of copper ($Cu2p_{3/2}$ and $Cu2p_{1/2}$) and silver ($Ag3d_{3/2}$ and $Ag3d_{5/2}$) were detected in the doped NTs, as shown in Fig. 2b and c, respectively, indicates clearly that Ag and Cu species are successfully incorporated into the oxide lattice during its growth.

Figure 3a shows high-resolution region scan spectra of the Ti2p for pure TiO_2 NTs. This spectrum is fitted with three peaks corresponding to titanium dioxide (Ti^{4+}) and titanium suboxide (Ti^{3+}) in $Ti2p_{1/2}$ and $Ti2p_{3/2}$, respectively. These peaks are fitted as $Ti^{4+}2p_{3/2}$ at 459.38 eV, $Ti^{4+}2p_{1/2}$ at 465.11 eV, and $Ti^{3+}2p_{3/2}$ at 460.87 eV. The position and the FWHM (~ 1.5 eV) of the observed peak at 460.87 eV are consistent with Ti^{4+} in the TiO_2 lattice [34, 35]. The difference between the energy of $Ti^{4+}2p_{1/2}$ and $Ti^{4+}2p_{3/2}$ is 5.73 eV, which is consistent with the standard binding energy of TiO_2 [34, 36, 37]. The $Ti^{3+}2p_{3/2}$ is attributed to the formation of Ti^{3+} and the presence of oxygen deficiency in TiO_2 NTs [22, 38]. After doping with Ag, the high-resolution XPS spectrum (Fig. 3b) shows a slight shift in the position along with a variation in the area of the peaks. The Ti2p spectrum is fitted with three peaks located at binding energies 458.65 eV ($Ti^{4+}2p_{3/2}$), 464.38 eV ($Ti^{4+}2p_{1/2}$), and 460.87 eV ($Ti^{3+}2p_{3/2}$), respectively. Figure 3c shows the high-resolution spectrum of Cu-TiO_2 NTs. Similar to Ag-doped TiO_2 NTs, the Ti2p spectrum is fitted with peaks at 459.04 eV ($Ti^{4+}2p_{3/2}$), 464.78 eV ($Ti^{4+}2p_{1/2}$), and 459.11 eV ($Ti^{3+}2p_{3/2}$), respectively. The shift of $Ti^{4+}2p$ peaks to lower binding energy for doped TiO_2 NTs is widely discussed in the literature. It has been explained by the formation of Ti^{3+} species or substitution of Ti^{+4} by Cu^+ and Ag^+ ions in Cu-TiO_2 NTs and Ag-TiO_2 NT samples, respectively [39–42]. In comparison to the pure TiO_2, the area of the Ti^{3+} peak in Ag-TiO_2 NTs and Cu-TiO_2 NT samples decreased, and that of the Ti^{4+} peak increased (Table 2). The increase in the area of Ti^{4+} peak after doping indicates that the doping improves the formation of TiO_2. These can be explained by the interaction between oxygen vacancies in TiO_2 NTs and the doped element.

The oxygen O1s peak of pure TiO_2 NTs (Fig. 4a) is prominent and can be deconvoluted into two subpeaks, centered at 530.67 eV and 532.41 eV. The first peak is attributed to the oxygen engaged in a Ti–O bond in TiO_2 or Ti_2O_3 lattice (O_L), while the second one is related to the H–O bond or the adsorbed oxygen type O_2 on the surface of TiO_2 (O_H) [34, 43–45]. Similarly, for the doped sample, the O1s spectrum of Cu and Ag-doped TiO_2 NTs fitted with two peaks is shown in Fig. 4b and c, respectively. However, in this case, the first peak air is higher than that of the second one. The increase in the area of the original peak at 530.67 eV after doping indicates that the doping may improve the formation of TiO_2.

Figure 5 shows the high-resolution XPS spectrum of Cu2p in Cu-TiO_2 NTs. In this spectrum, the doublet $Cu2p_{3/2}$

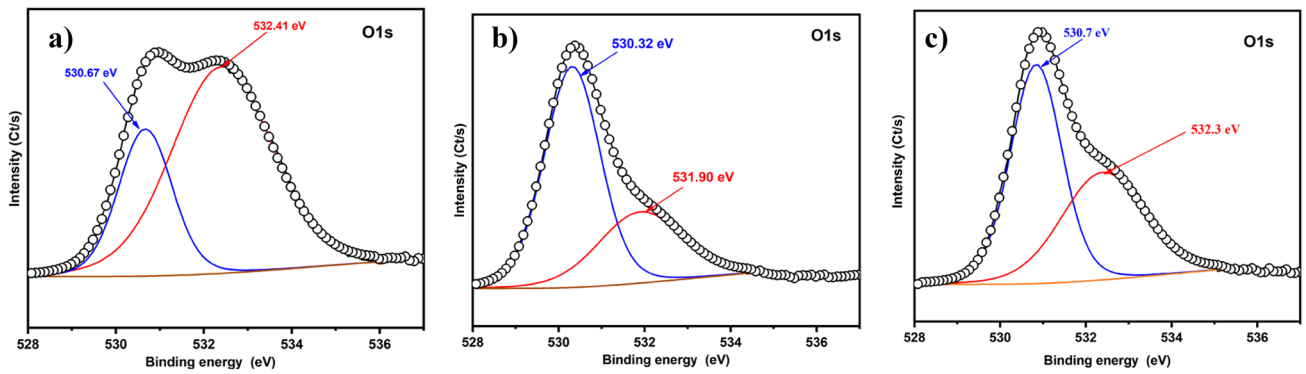

Fig. 4 Typical O1s spectra: **a** pure TiO_2 NTs, **b** Cu-doped TiO_2 NTs, and **c** Ag-doped TiO_2 NTs

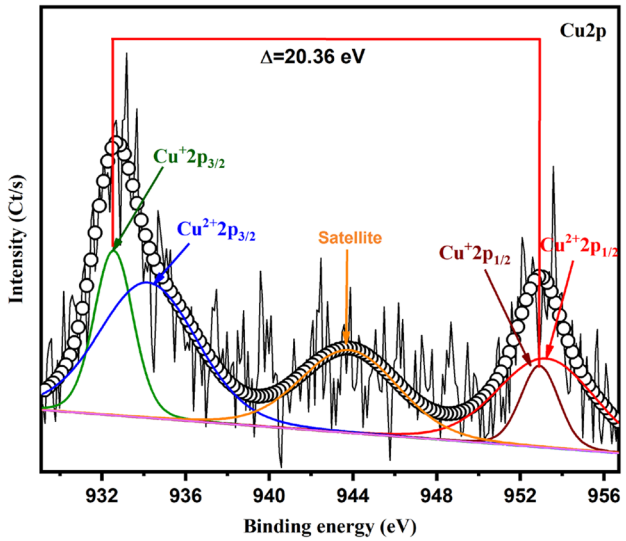

Fig. 5 High-resolution XPS spectra of Cu2p region for Cu-TiO_2 NTs

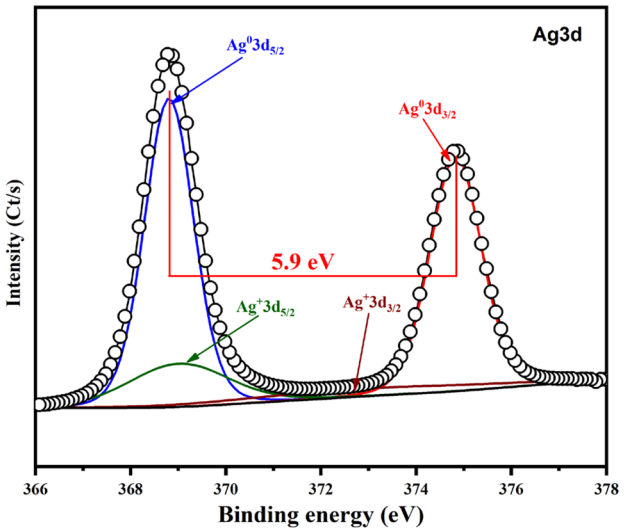

Fig. 6 High-resolution XPS spectra of Ag3d region for Ag-TiO_2 NTs

at 932.56 eV and $Cu2p_{1/2}$ at 952.92 eV arises from spin orbit-splitting. These peaks are related to Cu^+ [46, 47]. Also, the shoulders $Cu2p_{3/2}$ at binding energy 934.20 eV and $Cu2p_{1/2}$ at 953.23 eV are corresponding to Cu^{2+} [39, 46, 48]. The satellite peaks are also located at 943.93 eV [49]. This observation revealed that the doped Cu in the TiO_2 lattice is in a mixture of Cu^+ and Cu^{2+} oxidation states. The $Cu2p_{3/2}$ peak transition is lower than the values reported in the literature (933.6 eV) [50]. The shift of binding energies of $Cu2p_{3/2}$ peaks to the lower energy indicates the substitutional incorporation of Cu ions in the TiO_2 lattice rather than the formation of Cu_2O or/and CuO at the surface of TiO_2 [51–54].

For the Ag-TiO_2 NT sample, the XPS diagram of high resolution for Ag3d (Fig. 6) has two peaks at 368.8 eV and 374.7 eV, belonging to the $Ag3d_{5/2}$ and $Ag3d_{3/2}$ orbits [55], respectively. The splitting of Ag3d doublet at about 5.9 eV confirms that the Ag element is present as metallic silver (Ag^0) in the Ag-TiO_2 NT sample [56, 57], while the weak peaks at 367.7 and 373.7 eV are attributed to $Ag3d_{5/2}$ and $Ag3d_{3/2}$ of silver ions (Ag^+). These results further prove that Ag^0 and Ag^+ exist simultaneously on the surface of the Ag-TiO_2 NT sample [58, 59]. The oxygen deficiency can explain the formation of Ag^0 at the surface of TiO_2 [24, 60].

X-ray diffraction (XRD) pattern

Determination of crystal structure, phase composition, and crystallite size of the synthesized pure TiO_2 NTs, Cu-doped TiO_2 NTs, and Ag-doped TiO_2 NTs is carried out using XRD, and the results are shown in Fig. 7. The X-ray diffraction spectra of all the samples showed well-defined peaks, which could be indexed to the anatase, rutile phases of TiO_2, and titanium according to JCPDS file numbers 21–1272, 21–1276, and 44–1296, respectively. The peaks in pure TiO_2 NTs are attributed to the reflection from (101), (200), and (105) planes of the anatase. In addition, the rutile phase is revealed by the apparition of peaks at 27.4°, 36.07°, 41°, 43.6°, and 56.9° corresponding to planes (110) (101), (111), (210), and (220), respectively. However, the Cu and Ag peaks are not visible in the XRD spectra of the doped TiO_2 NTs. This is probably due to their low amount or their high dispersion in the samples with small dimensions below the detection limits of XRD. Xu et al. [61]. reported that the diffraction peaks of copper species disappeared when the copper component was highly dispersed in TiO_2. Compared to pure TiO_2 NTs, the anatase diffraction peak (200) shifts slightly to lower 2θ values in the Ag- and Cu-doped TiO_2 NTs (inset in Fig. 7). In addition, the intensity of doped TiO_2 NT peaks is higher than that of pure TiO_2 NTs, which indicates that the doping enhances the crystallinity and improves the structural quality of TiO_2 (according to XPS results). On the other hand, the peak intensity of (100) anatase plan in doped TiO_2 NTs is higher than pure TiO_2 samples, while the peak intensity of rutile decreases.

It is well known that the grain size and phase composition of TiO_2 are the most significant for a TiO_2 photocatalyst [32, 62–64]. From XRD data, the grain size was calculated using the Scherrer equation [65]. The crystallite sizes of pure TiO_2 NTs, Cu-doped TiO_2 NTs, and Ag-doped TiO_2 NTs ranged from 29.7 to 35.5 nm (pure TiO_2: 35.5 nm; Ag-TiO_2 NTs: 29.71 nm, and Cu-TiO_2 NTs: 29.71 nm). In addition, the relative anatase/rutile ratio was estimated at 56.25%/43.75%, 83%/17%, and 83%/17% in pure TiO_2 NTs, Cu-TiO_2 NTs, and Ag-TiO_2 NTs, respectively. These results

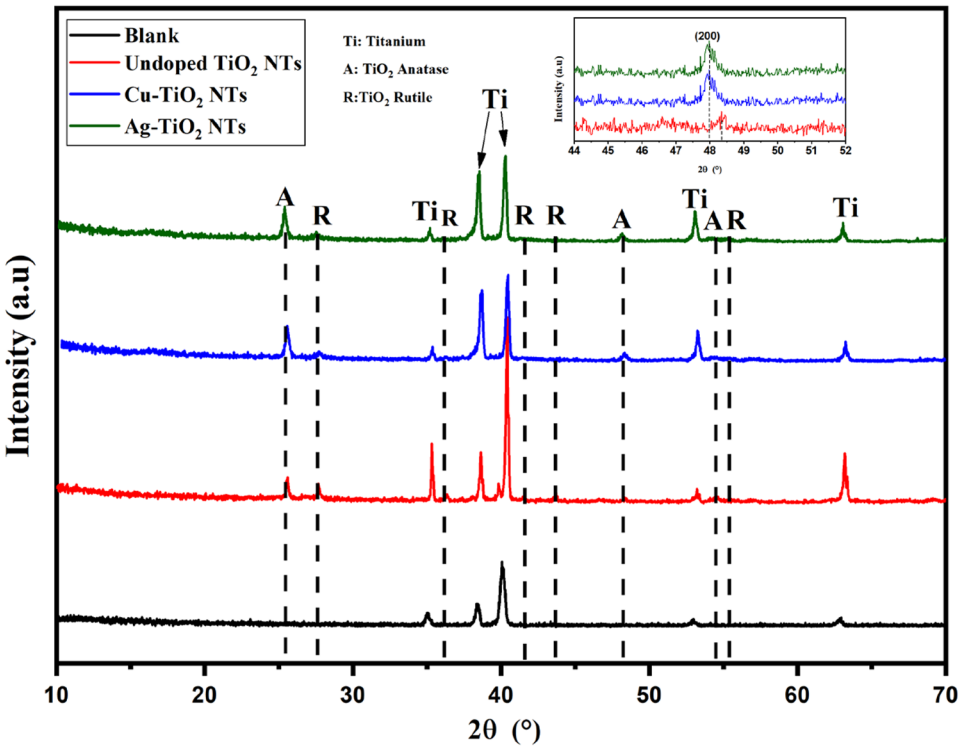

Fig. 7 XRD spectra of pure TiO_2 NTs, Cu-TiO_2 NTs, and Ag-TiO_2 NTs

indicate that Ag and Cu inhibit the anatase–rutile phase transformation and stabilize the anatase phase significantly compared to the rutile phase [66].

Raman spectroscopy

The Raman spectra obtained for pure and doped TiO_2 NTs are presented in Fig. 8. For all samples, the Raman spectra show six Raman-active modes (Eg, Eg, B1g, B1g + A1g, and Eg), which indicates that the samples consist of a mixture of anatase and rutile phases [31, 35, 67]. The characteristic Raman peaks at around 144.56, 197.8, 396.1, 516, and 638 cm^{-1} are indexed to E_g (1), E_g (2), B_{1g}, A_{1g}, and E_g (3) of anatase, respectively [31, 68]. Furthermore, the characteristic peaks of the rutile phase are observed at around 452 and 615 cm^{-1} [69]. The anatase band E_g (1) is shifted, from 143 cm^{-1} (for pure TiO_2) to 143.7 cm^{-1} for the doped samples (inset in Fig. 8). The shift of the anatase band (E_g (1)) has been reported in previous studies and attributed to the formation of Ti^{3+}, change of crystal size, and oxygen deficiencies in TiO_2 lattice [35, 70–74]. These results are consistent with those of XPS and XRD results.

FTIR analysis

The FT-IR spectra of pure and doped TiO_2 NTs calcined for 2 h at 600 °C are presented in Fig. 9. Compared with pure TiO_2 NTs, there are no differences in the FT-IR spectra of doped TiO_2 NTs. The figure shows the presence of some bands between 560 and 800 cm^{-1} which are attributed to different vibrational modes of anatase and rutile phases of TiO_2 [19, 75]. Especially, the intense band observed below at 620 cm^{-1} is due to Ti–O vibrations [19, 76, 77]. The band at around 1631 cm^{-1} is attributed to the stretching vibrations of the O–H groups at the TiO_2 surface. On the other hand, a slight shift in the position and the change in the intensity of bands are observed. These shift may be due to the presence of the dopants in the interstitials of the lattices of the

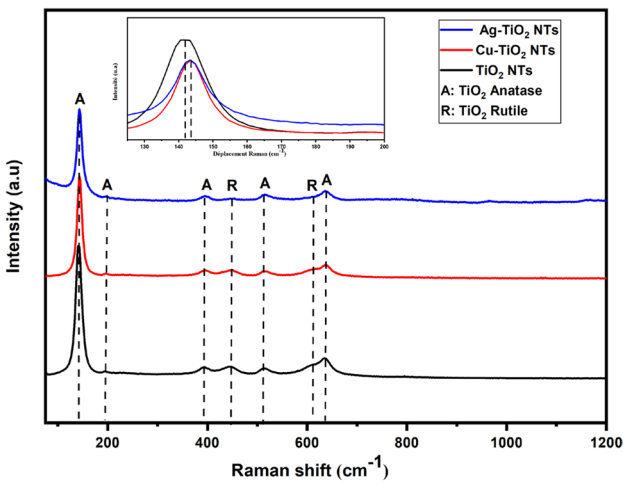

Fig. 8 Raman spectra of pure TiO_2 NTs, Cu-TiO_2 NTs, and Ag-TiO_2 NTs

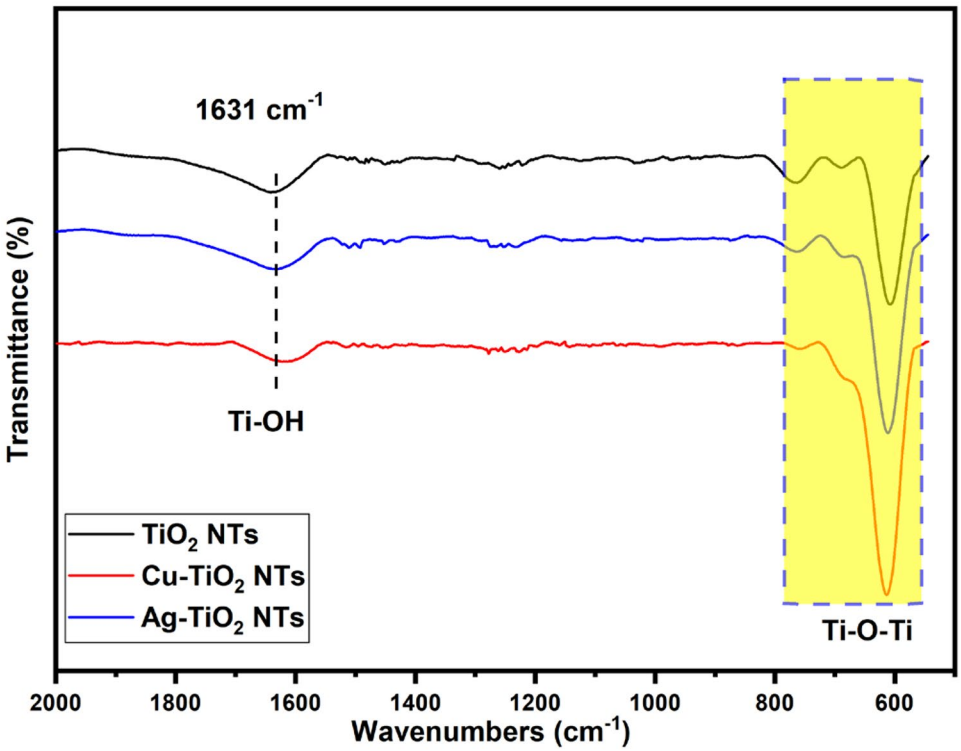

Fig. 9 FT-IR spectra of pure and doped TiO_2 NTs

doped samples [78]. These results are in agreement with those obtained by XRD and Raman analysis.

Mott-Schottky (MS) analysis

Determination of the semiconductor nature, the flat band positions (E_{FB}), and the carrier density (N_D) provide the first test that the material may be an effective photocatalyst. The most often used method for determining all these proprieties is based on measuring the potential dependence of the space charge region capacity (C_{sc}). Figure 10 shows the variation of C_{sc} for all samples as a function of the applied voltage in Mott-Schottky representation. The slope of all lines is positive, indicating that all investigated samples are an n-type semiconductor. Using the slope and intercept of the linear region, the N_D and E_{FB} were calculated according to the following Mott-Schottky relation [34, 79, 80].

$$\frac{1}{C_S^2} = \frac{2}{\varepsilon_0 \varepsilon_S e N_D}\left(E - E_{FB} - \frac{kT}{e}\right) \quad (1)$$

where C_S is the space charge layer capacitance, e is the electron charge (1.60 10^{-19} C), ε_0 is the permittivity of free space (8.85 10^{-14} F cm^{-1}), ε_S is the dielectric constant of TiO_2, which is assumed to be 100 F cm^{-1} [81], E is the applied potential, k is the Boltzmann constant (1.38 10^{23} J K^{-1}), and T is the absolute temperature.

The potential of the flat band (E_{FB}) shifts from − 0.19 V/SCE for pure TiO_2NTs to − 0.31 and − 0.46 V/SCE for Ag-TiO_2 NTs and Cu-TiO_2 NTs, respectively. On the other hand, the donor concentration N_D of about 4.50×10^{17}, 1.97×10^{17}, and 4.20×10^{17} cm^{-3} for pure TiO_2 NTs, Cu-TiO_2 NTs, and Ag-TiO_2 NTs, respectively.

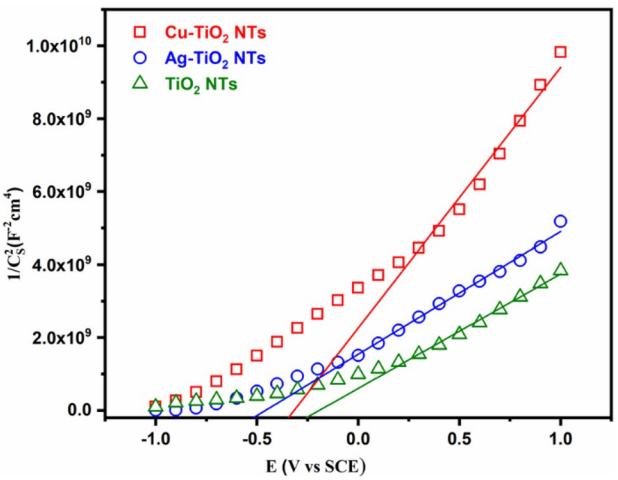

Fig. 10 MS plots of pure TiO_2 NTs, Cu-TiO_2 NTs, and Ag-TiO_2 NTs

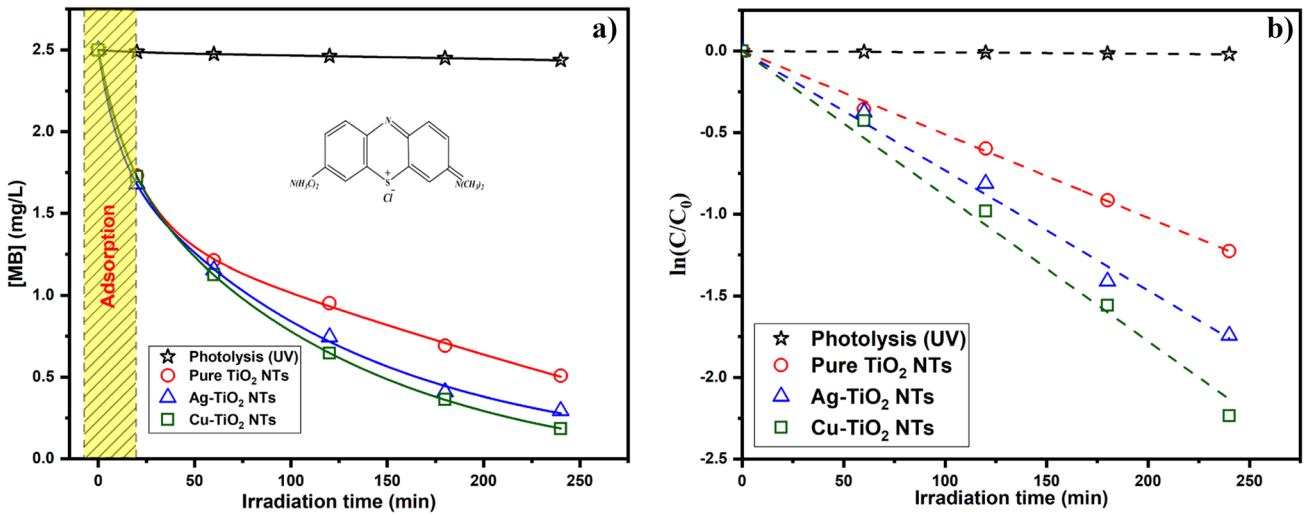

Fig. 11 Degradation of MB by photocatalysis on the pure TiO_2NTs, Ag-TiO_2 NTs, and Cu-TiO_2 NT surface, [MB] = 2.5 mg/L, Xe lamp 300 W

Photocatalytic activity

The photocatalytic capacity of all samples was evaluated by the photodegradation of MB under UV irradiation. Figure 11a shows the evolution of the methylene blue concentration ([MB]) versus the irradiation time in the presence of a different catalyst. Under UV irradiation and in the absence of TiO_2 (photolysis), the concentration of MB is kept constant, suggesting that the MB is stable under UV irradiation. However, in the simultaneous presence of TiO_2 and UV, the MB concentration decreases with the irradiation time, demonstrating it is degradation.

The experimental data of Fig. 11a were found to fit approximately a pseudo-first-order kinetic model by the linear transforms $\ln(C/C_0) = f(t) = kt$ [82, 83], as shown in Fig. 11b. The values of the rate constant (k), regression coefficient, and degradation efficiency (%) are listed in Table 3. The higher R^2 reveals that the decomposition kinetics essentially follows first-order kinetics. The results demonstrated that the Cu- and Ag-doped TiO_2 nanotube arrays exhibited a higher photocatalytic activity than the pure TiO_2 sample. From Table 3, only ~2.5% of MB is degraded by the photolysis process, about 79.6 9%, 88.23%, and 92.61% after 4 h of irradiation using pure TiO_2 NTs, Ag-TiO_2 NTs, and Cu-TiO_2 NTs, respectively. The higher efficiency of doped TiO_2 can be explained by the enhancement of charge separation of photogenerated electrons and holes on TiO_2 by doping.

A recent study showed that the inclusion of doped elements increased the photocatalytic activity of TiO_2 under UV irradiation. For comparison, a summary list of very recent studies on photodegradation of MB by different based TiO_2 photocatalyst is listed in Table 4. The degradation percentages obtained by doped TiO_2 NTs prepared in our conditions are very near to those reported in the literature for TiO_2 nanoparticles.

Previous studies demonstrate that the photocatalytic reaction pathway is believed to involve the reaction of MB with the generated $OH^{\bullet}$ radicals producing a range of intermediate products to reach complete mineralization with the formation of CO_2 and H_2O [82, 87–90]. To study the main active components in the degradation process of MB on the TiO_2 surface and to understand the degradation mechanism in more detail, trapping experiments were carried out. Isopropanol [91], triethanolamine [92], and benzoquinone [93, 94] are used as scavengers to capture hydroxyl radicals ($OH^{\bullet}$), photogenerated holes (h^+), and superoxide anion radical ($O2^{\bullet-}$), respectively.

Table 3 Photodegradation kinetics data of MB by TiO_2

Samples	k (min^{-1})	R^2	Degradation efficiency (%)
Photolysis	0.0001	0.98	2.5
Pure TiO_2 (TiO_2 NTs)	0.0051	0.99	79.69
Ag doped TiO_2 (Ag-TiO_2 NTs)	0.0073	0.99	88.23
Cu doped TiO_2 (Cu-TiO_2 NTs)	0.0089	0.99	92.61

Table 4 Photocatalytic activity of recently studied TiO_2-based photocatalysts for MB degradation under UV irradiation

Photocatalyst	Irradiation time (min)	Degradation efficiency (%)	Ref
Ag-doped TiO_2	360	94	[84]
Cu-doped TiO_2	300	93	[23]
Hg-doped TiO_2	120	56.72	[85]
Au-doped TiO_2	200	50	[24]
Zn-doped TiO_2	300	99	[23]
V_2O_5-doped TiO_2	120	92	[86]

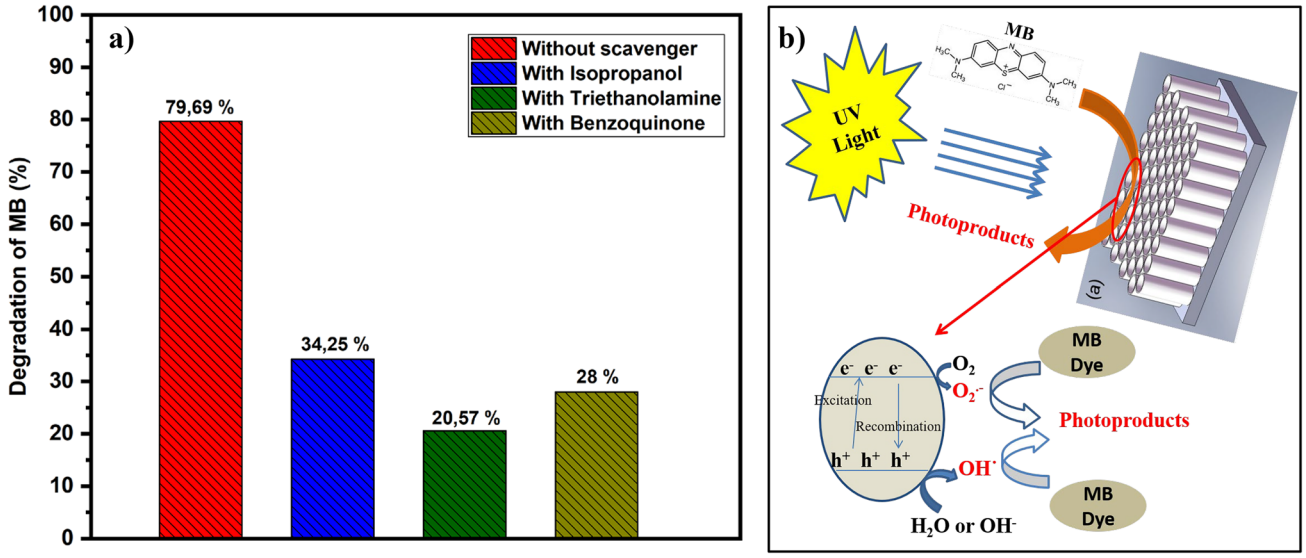

Fig. 12 Effects of radical scavenger addition on the photodegradation of MB **a** and schematic diagram of the photocatalytic mechanism of TiO_2 photocatalyst **b**

To demonstrate the involvement of these radicals, a mixture of MB and isopropanol (2% v/v) or triethanolamine (2% v/v) or benzoquinone (2% v/v) was irradiated under the same conditions. The results obtained are shown in Fig. 12. As can be observed in Fig. 12a, the addition of a radical scavenger inhibits the degradation of MB. These results indicate that holes are the primary active species in the degradation of MB, while $OH^{\bullet}$ and $O2^{\bullet-}$ radicals are likely of secondary importance in photodegradation.

Based on the above results and literature reports [95, 96], the possible photocatalytic mechanism of the TiO_2 NT photocatalyst was plotted as shown in Fig. 12b. The photodegradation process depends on the generation and separation of carriers; under light conditions, once the semiconductor absorbing

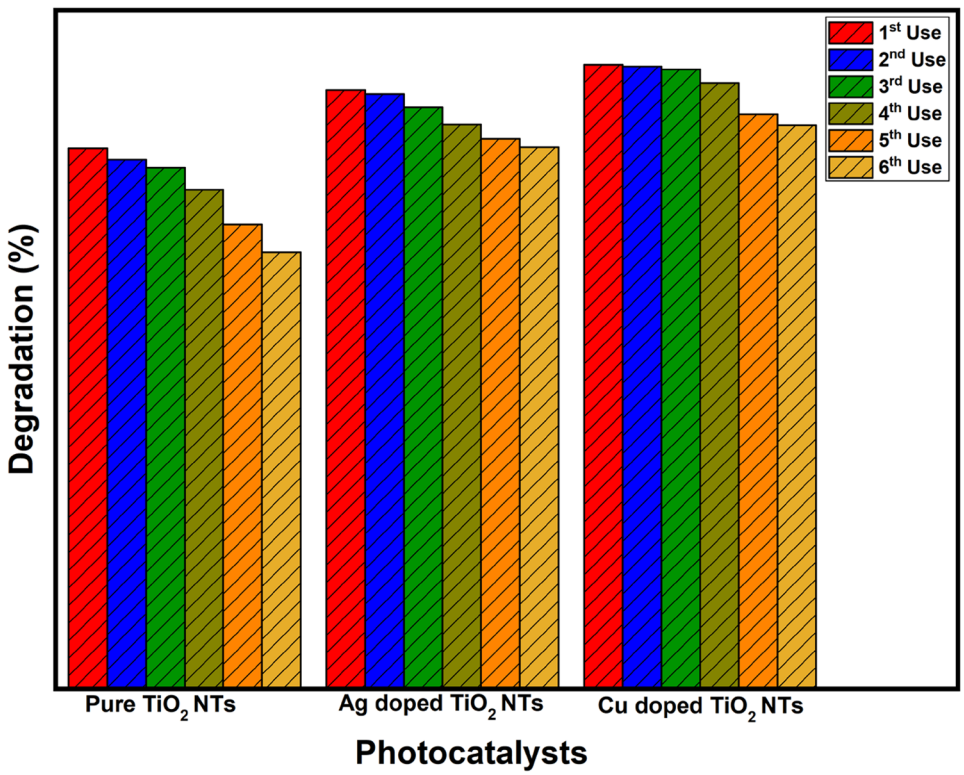

Fig. 13 Photocatalytic reusability efficiency of all photocatalysts up to six uses

energy is higher than the energy of its energy band, electrons will be excited from the valence band to the conduction band. At the same time, holes remain on the former (Eq. 2). According to the following equations, the formed holes reacted directly with MB molecules, H_2O, or OH^- adsorbed in the TiO_2 surface to form the active species ($OH^\bullet$) [6, 97–103].

$$TiO_2 + h\upsilon \rightarrow e^-_{CB} + h^+_{VB} \quad (2)$$

$$h^+_{VB} + H_2O \rightarrow +H^+ + OH^\cdot \quad (3)$$

$$h^+_{VB} + OH^- \rightarrow +TiO_2 + OH^\cdot \quad (4)$$

$$\text{MB Dye} + h^+_{VB} \rightarrow \text{Oxidation products} \quad (5)$$

Reusability efficiency

In addition to the photocatalytic efficiency of the TiO_2 NTs, the stability and the reusability of the TiO_2 NT photocatalyst are significant parameters to assess its practical application in wastewater treatment. Therefore, we carried out studies on the reutilization of the photocatalysts. After every use, the photocatalyst was washed with distilled water and ethanol and then dried for 30 min at 60 °C. The same procedure was repeated six times with the already used photocatalyst. The results obtained are represented in Fig. 13. The activity of all photocatalysts showed a gradual decrease. The degradation efficiencies of 64.35, 79.83, and 83.07% were achieved for pure TiO_2 NT, Ag-TiO_2 NT, and Cu-TiO_2 NT photocatalysts, respectively, after 6 reutilizations. These results indicate that the photocatalysts are globally stables and efficient for water treatment. This decrease in photocatalytic activity can be explained by poisoning of the active surface of the photocatalyst or the occupation of active sites by intermediates that adsorbed strongly on the surface of the photocatalyst [104, 105].

Conclusion

A facile and novel one-step anodization process fabricated photocatalytic materials based on copper- and silver-doped TiO_2 NTs. The obtained NTs have a diameter and wall thickness of 128 and 56 nm, respectively. The Cu-doped TiO_2 NT composites have excellent photocatalytic performance. Copper doping improved the photocatalytic performance of TiO_2 NTs. These NTs are exciting candidates for photocatalytic reactions, such as MB oxidation. The new anodization process developed in this study is a simple and efficient method that can be easily scaled up, thereby pioneering the fabrication of high-performance metal-doped TiO_2 NT photocatalysts with promising environmental applications.

Acknowledgements The authors are grateful to the Centre of Analysis and Characterization (CAC) of the Faculty of Sciences Semlalia in Marrakesh for the research facilities and the National Center for Scientific and Technical Research (CNRST) in Rabat for its financial support.

References

1. Gorduk S, Avciata O, Avciata U (2021) Hydrothermal in situ preparation of phthalocyanine–TiO_2 nanocomposites for photocatalytic activity under visible light irradiation. Res Chem Intermed 47:615–635. https://doi.org/10.1007/s11164-020-04289-3
2. Tahir M, Tahir B, Amin NAS (2015) Gold-nanoparticle-modified TiO_2 nanowires for plasmon-enhanced photocatalytic CO_2 reduction with H_2 under visible light irradiation. Appl Surf Sci 356:1289–1299. https://doi.org/10.1016/j.apsusc.2015.08.231
3. Wu Y, Long M, Cai W et al (2009) Preparation of photocatalytic anatase nanowire films by in situ oxidation of titanium plate. Nanotechnology 20. https://doi.org/10.1088/0957-4484/20/18/185703
4. Kočí K, Obalová L, Matějová L et al (2009) Effect of TiO_2 particle size on the photocatalytic reduction of CO_2. Appl Catal B Environ 89:494–502. https://doi.org/10.1016/j.apcatb.2009.01.010
5. Yang Y, Qiu M, Liu L (2016) TiO_2 nanorod array@carbon cloth photocatalyst for CO_2 reduction. Ceram Int 42:15081–15086. https://doi.org/10.1016/j.ceramint.2016.06.020
6. Xu H, Ouyang S, Li P et al (2013) High-active anatase TiO_2 nanosheets exposed with 95% 100 facets toward efficient H2 evolution and CO2 photoreduction". ACS Appl Mater Interfaces 5:8262. https://doi.org/10.1021/am402298g
7. Cheng J, Zhang M, Wu G et al (2014) Photoelectrocatalytic reduction of CO_2 into chemicals using Pt-modified reduced graphene oxide combined with Pt-modified TiO_2 nanotubes. Environ Sci Technol 48:7076–7084. https://doi.org/10.1021/es500364g
8. Fang B, Bonakdarpour A, Reilly K et al (2014) Large-scale synthesis of TiO_2 microspheres with hierarchical nanostructure for highly efficient photodriven reduction of CO_2 to CH_4. ACS Appl Mater Interfaces 6:15488–15498. https://doi.org/10.1021/am504128t
9. Pomoni K, Vomvas A, Trapalis C (2008) Electrical conductivity and photoconductivity studies of TiO_2 sol-gel thin films and the effect of N-doping. J Non Cryst Solids 354:4448–4457. https://doi.org/10.1016/j.jnoncrysol.2008.06.069
10. Humayun M, Raziq F, Khan A, Luo W (2018) Modification strategies of TiO_2 for potential applications in photocatalysis: a critical review. Green Chem Lett Rev 11:86–102. https://doi.org/10.1080/17518253.2018.1440324
11. Choi W, Termin A, Hoffmann MR (1994) The role of metal ion dopants in quantum-sized TiO2: correlation between photoreactivity and charge carrier recombination dynamics. J Phys Chem 98:13669–13679. https://doi.org/10.1021/j100102a038
12. Ghicov A, Schmidt B, Kunze J, Schmuki P (2007) Photoresponse in the visible range from Cr doped TiO_2 nanotubes. Chem Phys Lett 433:323–326. https://doi.org/10.1016/j.cplett.2006.11.065
13. Srinivas B, Shubhamangala B, Lalitha K et al (2011) Photocatalytic reduction of CO_2 over Cu- TiO_2/ molecular sieve 5A composite. Photochem Photobiol 87:995–1001. https://doi.org/10.1111/j.1751-1097.2011.00946.x
14. Chong B, Zhu W, Hou X (2017) Epitaxial hetero-structure of CdSe/ TiO_2 nanotube arrays with PEDOT as a hole transfer layer for photoelectrochemical hydrogen evolution. J Mater Chem A 5:6233–6244. https://doi.org/10.1039/c6ta10202f

15. Lana-villarreal T, Bisquert J (2009) CdSe quantum dot-sensitized TiO_2 electrodes : effect of quantum dot coverage and mode Ne. 4208–4214
16. Hou Y, Li X, Zou X et al (2009) Photoeletrocatalytic activity of a Cu_2O-loaded self-organized highly oriented TiO_2 nanotube array electrode for 4-chlorophenol degradation. 43:858–863
17. Shen K, Wu K, Wang D (2014) Band alignment of ultra-thin hetero-structure ZnO/ TiO_2 junction. Mater Res Bull 51:141–144. https://doi.org/10.1016/j.materresbull.2013.12.013
18. Davaslıoğlu İÇ, Volkan Özdokur K, Koçak S et al (2021) WO3 decorated TiO_2 nanotube array electrode: preparation, characterization and superior photoelectrochemical performance for rhodamine B dye degradation. J Mol Struct 1241. https://doi.org/10.1016/j.molstruc.2021.130673
19. Gorduk S, Avciata O, Avciata U (2018) Photocatalytic degradation of methylene blue under visible light irradiation by non-peripherally tetra substituted phthalocyanine- TiO_2 nanocomposites. Inorganica Chim Acta 471:137–147. https://doi.org/10.1016/j.ica.2017.11.004
20. Avciata O, Benli Y, Gorduk S, Koyun O (2016) Ag doped TiO_2 nanoparticles prepared by hydrothermal method and coating of the nanoparticles on the ceramic pellets for photocatalytic study: Surface properties and photoactivity. J Eng Technol Appl Sci 1:34–50. https://doi.org/10.30931/jetas.281381
21. Khalid NR, Ahmed E, Hong Z et al (2013) Cu-doped TiO_2 nanoparticles/graphene composites for efficient visible-light photocatalysis. Ceram Int 39:7107–7113. https://doi.org/10.1016/j.ceramint.2013.02.051
22. Carvalho HWP, Rocha MVJ, Hammer P, Ramalho TC (2013) TiO_2-Cu photocatalysts: a study on the long- and short-range chemical environment of the dopant. J Mater Sci 48:3904–3912. https://doi.org/10.1007/s10853-013-7192-1
23. Park JY, Il CK, Lee JH et al (2013) Fabrication and characterization of metal-doped TiO_2 nanofibers for photocatalytic reactions. Mater Lett 97:64–66. https://doi.org/10.1016/j.matlet.2013.01.047
24. Sangpour P, Hashemi F, Moshfegh AZ (2010) Photoenhanced degradation of methylene blue on cosputtered M: TiO_2 (M = Au, Ag, Cu) nanocomposite systems: a comparative study. J Phys Chem C 114:13955–13961. https://doi.org/10.1021/jp910454r
25. Hahn R, Stark M, Killian MS, Schmuki P (2013) Photocatalytic properties of in situ doped TiO_2-nanotubes grown by rapid breakdown anodization. Catal Sci Technol 3:1765–1770. https://doi.org/10.1039/c3cy00021d
26. Momeni MM, Ghayeb Y, Ghonchegi Z (2015) Fabrication and characterization of copper doped TiO_2 nanotube arrays by in situ electrochemical method as efficient visible-light photocatalyst. Ceram Int 41:8735–8741. https://doi.org/10.1016/j.ceramint.2015.03.094
27. Vásquez-García SR, Garcia-Rueda AK, Flores-Ramírez N et al (2018) Synthesis and characterization of TiO_2 nanotubes doped with Fe via in situ Anodization. J Mater Sci Mater Electron 29:15814–15820. https://doi.org/10.1007/s10854-018-9339-y
28. Husin Milad AM, Minggu LJ, Kassim MB, Daud WRW (2013) Carbon doped TiO_2 nanotubes photoanodes prepared by in-situ anodic oxidation of Ti-foil in acidic and organic medium with photocurrent enhancement. Ceram Int 39:3731–3739. https://doi.org/10.1016/j.ceramint.2012.10.209
29. Mishra T, Wang L, Hahn R, Schmuki P (2014) In-situ Cr doped anodized TiO_2 nanotubes with increased photocurrent response. Electrochim Acta 132:410–415. https://doi.org/10.1016/j.electacta.2014.03.101
30. Zhao S, Xing J, Fan H et al (2017) Derivation of a mathematical model for the growth of anodic TiO_2 nanotubes under constant current conditions. J Electrochem Soc 164:E187–E193. https://doi.org/10.1149/2.0421709jes
31. Zakir O, Idouhli R, Elyaagoubi M et al (2020) Fabrication of TiO_2 nanotube by electrochemical anodization: toward photocatalytic application. J Nanomater 2020. https://doi.org/10.1155/2020/4745726
32. Zakir O, mountassir El Mouchtari E, Elyaagoubi M et al (2022) Anodic TiO_2 nanotube: influence of annealing temperature on the photocatalytic degradation of carbamazepine. J Aust Ceram Soc. https://doi.org/10.1007/s41779-022-00752-z
33. Ge H, Tian H, Zhou Y et al (2014) Influence of surface states on the evaluation of the flat band potential of TiO_2. ACS Appl Mater Interfaces 6:2401–2406. https://doi.org/10.1021/am404743a
34. Khadiri M, Elyaagoubi M, Idouhli R et al (2020) Electrochemical study of anodized titanium in phosphoric acid. Adv Mater Sci Eng 2020:1–11. https://doi.org/10.1155/2020/5769071
35. Zhang H, Xing Z, Zhang Y et al (2015) Ni^{2+} and Ti^{3+} co-doped porous black anatase TiO_2 with unprecedented-high visible-light-driven photocatalytic degradation performance. RSC Adv 5:107150–107157. https://doi.org/10.1039/c5ra23743b
36. Ohashi Y, Nagatsuka N, Ogura S, Fukutani K (2019) Hydrogen distribution and electronic structure of TiO_2 (110) hydrogenated with low-energy hydrogen ions. J Phys Chem C 123:10319–10324. https://doi.org/10.1021/acs.jpcc.8b09434
37. Georgios P, Wolfgang SM (2010) X-ray photoelectron spectroscopy of anatase- TiO_2 coated carbon nanotubes. Solid State Phenom 162:163–177. https://doi.org/10.4028/www.scientific.net/SSP.162.163
38. Deng G, Xanthopoulos N, Muralt P (2008) Chemical nature of colossal dielectric constant of $CaCu_3Ti_4O_{12}$ thin film by pulsed laser deposition. Appl Phys Lett 92:3–6. https://doi.org/10.1063/1.2919076
39. Kashale AA, Dwivedi PK, Sathe BR et al (2018) Biomass-mediated synthesis of Cu-doped TiO_2 nanoparticles for improved-performance lithium-ion batteries. ACS Omega 3:13676–13684. https://doi.org/10.1021/acsomega.8b01903
40. Gao Q, Si F, Zhang S et al (2019) Hydrogenated F-doped TiO_2 for photocatalytic hydrogen evolution and pollutant degradation. Int J Hydrogen Energy 44:8011–8019. https://doi.org/10.1016/j.ijhydene.2019.01.233
41. Bharti B, Kumar S, Lee HN, Kumar R (2016) Formation of oxygen vacancies and Ti^{3+} state in TiO_2 thin film and enhanced optical properties by air plasma treatment. Sci Rep 6:1–12. https://doi.org/10.1038/srep32355
42. Md Saad SK, Ali Umar A, Ali Umar MI et al (2018) Two-dimensional, hierarchical Ag-doped TiO_2 nanocatalysts: effect of the metal oxidation state on the photocatalytic properties. ACS Omega 3:2579–2587. https://doi.org/10.1021/acsomega.8b00109
43. He X, Li S, Cao G et al (2020) In situ atomic-scale engineering of the chemistry and structure of the grain boundaries region of $Li_3xLa_{2/3-x}TiO_3$. Scr Mater 185:134–139. https://doi.org/10.1016/j.scriptamat.2020.04.018
44. Liu H, Liu G, Zhou Q (2009) Preparation and characterization of Zr doped TiO_2 nanotube arrays on the titanium sheet and their enhanced photocatalytic activity. J Solid State Chem 182:3238–3242. https://doi.org/10.1016/j.jssc.2009.09.016
45. Jiao S, Lian G, Jing L et al (2018) Sn-doped rutile TiO_2 hollow nanocrystals with enhanced lithium-ion batteries performance. ACS Omega 3:1329–1337. https://doi.org/10.1021/acsomega.7b01340
46. Wang Y, Duan W, Liu B et al (2014) The effects of doping copper and mesoporous structure on photocatalytic properties of TiO_2. J Nanomater 2014. https://doi.org/10.1155/2014/178152
47. Jiang L, Yao H, Luo X et al (2020) Polydopamine-modified copper-doped titanium dioxide nanotube arrays for copper-catalyzed controlled endogenous nitric oxide release and improved re-endothelialization. ACS Appl Bio Mater 3:3123–3136. https://doi.org/10.1021/acsabm.0c00157

48. Navas J, Sánchez-Coronilla A, Aguilar T et al (2014) Experimental and theoretical study of the electronic properties of Cu-doped anatase TiO_2. Phys Chem Chem Phys 16:3835–3845. https://doi.org/10.1039/c3cp54273d
49. Sun H, Zelekew OA, Chen X et al (2019) A noble bimetal oxysulfide CuVOS catalyst for highly efficient catalytic reduction of 4-nitrophenol and organic dyes. RSC Adv 9:31828–31839. https://doi.org/10.1039/C9RA05172D
50. Chusuei CC, Brookshier MA, Goodman DW (1999) Correlation of relative X-ray photoelectron spectroscopy shake-up intensity with CuO particle size. Langmuir 15:2806–2808. https://doi.org/10.1021/la9815446
51. Anitha B, Khadar MA (2016) Dopant concentration dependent magnetism of Cu-doped TiO_2 nanocrystals. J Nanoparticle Res 18:1–14. https://doi.org/10.1007/s11051-016-3464-4
52. Xin B, Wang P, Ding D et al (2008) Effect of surface species on Cu-TiO_2 photocatalytic activity. Appl Surf Sci 254:2569–2574. https://doi.org/10.1016/j.apsusc.2007.09.002
53. Li G, Dimitrijevic NM, Chen L et al (2008) Role of surface/interfacial Cu^{2+} sites in the photocatalytic activity of coupled CuO-TiO_2 nanocomposites. J Phys Chem C 112:19040–19044. https://doi.org/10.1021/jp8068392
54. Colón G, Maicu M, Hidalgo MC, Navío JA (2006) Cu-doped TiO_2 systems with improved photocatalytic activity. Appl Catal B Environ 67:41–51. https://doi.org/10.1016/j.apcatb.2006.03.019
55. Yang D, Sun Y, Tong Z et al (2015) Synthesis of Ag/ TiO_2 nanotube heterojunction with improved visible-light photocatalytic performance inspired by bioadhesion. J Phys Chem C 119:5827–5835. https://doi.org/10.1021/jp511948p
56. Xu L, Steinmiller EMP, Skrabalak SE (2012) Achieving synergy with a potential photocatalytic Z-scheme: synthesis and evaluation of nitrogen-doped TiO_2/SnO_2 composites. J Phys Chem C 116:871–877. https://doi.org/10.1021/jp208981h
57. Zhang J, Li X, Peng M et al (2018) Ag-doped TiO_2 hollow microspheres with visible light response by template-free route for removal of tetracycline hydrochloride from aqueous solution. Mater Res Express 5. https://doi.org/10.1088/2053-1591/aac66a
58. Ferraria AM, Carapeto AP, Botelho Do Rego AM (2012) X-ray photoelectron spectroscopy: silver salts revisited. Vacuum 86:1988–1991. https://doi.org/10.1016/j.vacuum.2012.05.031
59. Hakouk K, Deniard P, Lajaunie L et al (2013) Novel soft-chemistry route of $Ag_2Mo_3O_{10}{\cdot}2H_2O$ nanowires and in situ photogeneration of a $Ag@Ag_2Mo_3O_{10}{\cdot}2H_2O$ plasmonic heterostructure. Inorg Chem 52:6440–6449. https://doi.org/10.1021/ic400343v
60. Lee S (2004) Photocatalytic nanocomposite based on TiO_2 and carbon nanotubes. university of florida
61. Xu B, Dong L, Chen Y (1998) Influence of CuO loading on dispersion and reduction behavior of CuO/ TiO_2 (anatase) system. 94:1905–1909
62. Bacsa RR, Kiwi J (1998) Effect of rutile phase on the photocatalytic properties of nanocrystalline titania during the degradation of p -coumaric acid. 16:19–29
63. Bakardjieva S, Šubrt J, Štengl V et al (2005) Photoactivity of anatase-rutile TiO_2 nanocrystalline mixtures obtained by heat treatment of homogeneously precipitated anatase. Appl Catal B Environ 58:193–202. https://doi.org/10.1016/j.apcatb.2004.06.019
64. Tayade RJ, Surolia PK, Kulkarni RG, Jasra RV (2007) Photocatalytic degradation of dyes and organic contaminants in water using nanocrystalline anatase and rutile TiO_2. Sci Technol Adv Mater 8:455–462. https://doi.org/10.1016/j.stam.2007.05.006
65. Manickam K, Muthusamy V, Manickam S et al (2019) Effect of annealing temperature on structural, morphological and optical properties of nanocrystalline TiO_2 thin films synthesized by sol-gel dip coating method. Mater Today Proc 23:68–72. https://doi.org/10.1016/j.matpr.2019.06.651
66. Kim SG, Ju MJ, Choi IT et al (2013) Nb-doped TiO_2 nanoparticles for organic dye-sensitized solar cells. RSC Adv 16380–16386. https://doi.org/10.1039/C3RA42081G
67. Roy N, Sohn Y, Leung KT, Pradhan D (2014) Engineered electronic states of transition metal doped TiO_2 nanocrystals for low overpotential oxygen evolution reaction. J Phys Chem C 118:29499–29506. https://doi.org/10.1021/jp508445t
68. Siuzdak K, Szkoda M, Lisowska-Oleksiak A et al (2015) Thin layer of ordered boron-doped TiO_2 nanotubes fabricated in a novel type of electrolyte and characterized by remarkably improved photoactivity. Appl Surf Sci 357:942–950. https://doi.org/10.1016/j.apsusc.2015.09.130
69. Romanos GE, Athanasekou CP, Likodimos V et al (2013) Hybrid ultra filtration / photocatalytic membranes for efficient water treatment. Ind Eng Chem Res 52:13938–13947
70. Ekoi EJ, Gowen A, Dorrepaal R, Dowling DP (2019) Characterisation of titanium oxide layers using Raman spectroscopy and optical profilometry: influence of oxide properties. Results Phys 12:1574–1585. https://doi.org/10.1016/j.rinp.2019.01.054
71. Fagan R, McCormack DE, Hinder S, Pillai SC (2016) Improved high temperature stability of anatase TiO_2 photocatalysts by N, F, P co-doping. Mater Des 96:44–53. https://doi.org/10.1016/j.matdes.2016.01.142
72. Gupta SK, Desai R, Jha PK et al (2010) Titanium dioxide synthesized using titanium chloride: size effect study using Raman spectroscopy and photoluminescence. J Raman Spectrosc 41:350–355. https://doi.org/10.1002/jrs.2427
73. Carmichael P, Hazafy D, Bhachu DS et al (2013) Atmospheric pressure chemical vapour deposition of boron doped titanium dioxide for photocatalytic water reduction and oxidation. Phys Chem Chem Phys 15:16788–16794. https://doi.org/10.1039/c3cp52665h
74. Parker JC, Siegel RW (1990) Raman microprobe study of nanophase TiO_2 and oxidation-induced spectral changes. J Mater Res 5:1246–1252. https://doi.org/10.1557/JMR.1990.1246
75. Ganesh I, Gupta AK, Kumar PP et al (2012) Preparation and characterization of Ni-doped TiO_2 materials for photocurrent and photocatalytic applications. Sci World J 2012:13–20. https://doi.org/10.1100/2012/127326
76. Olgun U, Gülfen M, Üstel F, Arslan H (2018) Electro-optics and band gap energies of nanosilver-coated TiO_2 nanotubes on titanium metal. Acta Metall Sin English Lett 31:153–163. https://doi.org/10.1007/s40195-017-0664-6
77. Ganesh I, Kumar P, Gupta A et al (2012) Preparation and characterization of Fe-doped TiO_2 powders for solar light response and photocatalytic applications. Process Appl Ceram 6:21–36. https://doi.org/10.2298/pac1201021g
78. Raguram T, Rajni KS (2019) Synthesis and analysing the structural, optical, morphological, photocatalytic and magnetic properties of TiO_2 and doped (Ni and Cu) TiO_2 nanoparticles by sol–gel technique. Appl Phys A Mater Sci Process 125:1–11. https://doi.org/10.1007/s00339-019-2581-1
79. Radecka M, Rekas M, Trenczek-Zajac A, Zakrzewska K (2008) Importance of the band gap energy and flat band potential for application of modified TiO_2 photoanodes in water photolysis. J Power Sources 181:46–55. https://doi.org/10.1016/j.jpowsour.2007.10.082
80. Aljohani TA, Almutairi AK (2016) High photoconversion efficiency obtained from novel TiO_2 photoanodes. Int J Electrochem Sci 11:6848–6861. https://doi.org/10.20964/2016.08.22
81. Pu P, Cachet H, Sutter EMM (2010) Electrochemical impedance spectroscopy to study photo - induced effects on self-organized TiO_2 nanotube arrays. Electrochim Acta 55:5938–5946. https://doi.org/10.1016/j.electacta.2010.05.048
82. Gomes da Silva C, Faria JL (2003) Photochemical and photocatalytic degradation of an azo dye in aqueous solution by UV irradiation.

J Photochem Photobiol A Chem 155:133–143. https://doi.org/10.1016/s1010-6030(02)00374-x
83. Fu H, Quan X, Zhao H (2005) Photodegradation of γ-HCH by α-Fe_2O_3 and the influence of fulvic acid. J Photochem Photobiol A Chem 173:143–149. https://doi.org/10.1016/j.jphotochem.2005.01.013
84. Harikishore M, Sandhyarani M, Venkateswarlu K et al (2014) Effect of Ag doping on antibacterial and photocatalytic activity of nanocrystalline TiO_2. Procedia Mater Sci 6:557–566. https://doi.org/10.1016/j.mspro.2014.07.071
85. Abbas F, Bensaha R (2021) Effect of annealing time on structural and optical proprieties of mercury (Hg^{+2}) doped TiO_2 thin films elaborated by sol-gel method for future photo-catalytic application. Optik (Stuttg) 247:167846. https://doi.org/10.1016/j.ijleo.2021.167846
86. Bayati MR, Golestani-Fard F, Moshfegh AZ (2010) Photo-degradation of methelyne blue over V_2O_5- TiO_2 nano-porous layers synthesized by micro arc oxidation. Catal Letters 134:162–168. https://doi.org/10.1007/s10562-009-0231-5
87. Vamathevan V, Amal R, Beydoun D et al (2002) Photocatalytic oxidation of organics in water using pure and silver-modified titanium dioxide particles. J Photochem Photobiol A Chem 148:233–245. https://doi.org/10.1016/S1010-6030(02)00049-7
88. Zhang T, Oyama T, Aoshima A et al (2001) Photooxidative N-demethylation of methylene blue in aqueous TiO_2 dispersions under UV irradiation. J Photochem Photobiol A Chem 140:163–172. https://doi.org/10.1016/S1010-6030(01)00398-7
89. Jang HD, Kim SK, Kim SJ (2001) Effect of particle size and phase composition of titanium dioxide nanoparticles on the photocatalytic properties. J Nanoparticle Res 3:141–147. https://doi.org/10.1023/A:1017948330363
90. Zulmajdi SLN, Ajak SNFH, Hobley J et al (2017) Kinetics of photocatalytic degradation of methylene blue in aqueous dispersions of TiO_2 nanoparticles under UV-LED irradiation. Am J Nanomater 5:1–6. https://doi.org/10.12691/AJN-5-1-1
91. Yoon SH, Lee JH (2005) Oxidation mechanism of As(III) in the UV/ TiO_2 system: evidence for a direct hole oxidation mechanism. Environ Sci Technol 39:9695–9701. https://doi.org/10.1021/es051148r
92. Yan SC, Li ZS, Zou ZG (2010) Photodegradation of rhodamine B and methyl orange over boron-doped g-C3N4 under visible light irradiation. Langmuir 26:3894–3901. https://doi.org/10.1021/la904023j
93. Xue C, Zhang T, Ding S et al (2017) Anchoring tailored low-index faceted BiOBr nanoplates onto TiO_2 nanorods to enhance the stability and visible-light-driven catalytic activity. ACS Appl Mater Interfaces 9:16091–16102. https://doi.org/10.1021/acsami.7b00433
94. Kedves EZ, Pap Z, Hernadi K, Baia L (2021) Significance of the surface and bulk features of hierarchical TiO_2 in their photocatalytic properties. Ceram Int 47:7088–7100. https://doi.org/10.1016/j.ceramint.2020.11.061
95. Zhou Q, Zhang L, Zuo P et al (2018) Enhanced photocatalytic performance of spherical BiOI/MnO_2 composite and mechanism investigation. RSC Adv 8:36161–36166. https://doi.org/10.1039/c8ra06930a
96. Gao M, Zhang D, Pu X et al (2015) Facile hydrothermal synthesis of Bi/BiOBr composites with enhanced visible-light photocatalytic activities for the degradation of rhodamine B. Sep Purif Technol 154:211–216. https://doi.org/10.1016/j.seppur.2015.09.063
97. Zhu Z, Cai H, Sun DW (2018) Titanium dioxide (TiO_2) photocatalysis technology for nonthermal inactivation of microorganisms in foods. Trends Food Sci Technol 75:23–35. https://doi.org/10.1016/j.tifs.2018.02.018
98. Al-Mamun MR, Kader S, Islam MS, Khan MZH (2019) Photocatalytic activity improvement and application of UV-TiO_2 photocatalysis in textile wastewater treatment: a review. J Environ Chem Eng 7. https://doi.org/10.1016/j.jece.2019.103248
99. Mirkhani V, Tangestaninejad S, Moghadam M, Habibi MH (2009) Photocatalytic degradation of azo dyes catalyzed by Ag doped TiO_2 photocatalyst. 6:578–587
100. Tanaka K, Padermpole K, Hisanaga T (2000) Photocatalytic degradation of commercial azo dyes. Water Res 34:
101. Houas A, Lachheb H, Ksibi M et al (2001) Photocatalytic degradation pathway of methylene blue in water. Appl Catal B Environ 31:145–157
102. Prevot AB, Baiocchi C, Brussino MC et al (2001) Photocatalytic degradation of acid blue 80 in aqueous solutions containing TiO_2 suspensions. 971–976
103. Nasikhudin, Diantoro M, Kusumaatmaja A, Triyana K (2018) Study on photocatalytic properties of TiO_2 nanoparticle in various pH condition. J Phys Conf Ser 1011. https://doi.org/10.1088/1742-6596/1011/1/012069
104. Liu Y, Yu H, Lv Z et al (2012) Simulated-sunlight-activated photocatalysis of methylene blue using cerium-doped SiO_2/ TiO_2 nanostructured fibers. J Environ Sci (China) 24:1867–1875. https://doi.org/10.1016/S1001-0742(11)61008-5
105. Rao KVS, Subrahmanyam M, Boule P (2004) Immobilized TiO_2 photocatalyst during long-term use: decrease of its activity. Appl Catal B Environ 49:239–249. https://doi.org/10.1016/j.apcatb.2003.12.017